ACS Sustainable Chemistry & Engineering

Research Article

pubs.acs.org/journal/ascecg

Ultrafine Ni–Pt Alloy Nanoparticles Grown on Graphene as Highly Efficient Catalyst for Complete Hydrogen Generation from Hydrazine Borane

Zhujun Zhang, Zhang-Hui Lu,* and Xiangshu Chen

Jiangxi Inorganic Membrane Materials Engineering Research Centre, College of Chemistry and Chemical Engineering, Jiangxi Normal University, Nanchang 330022, China

Supporting Information

ABSTRACT: Ultrafine Ni–Pt alloy NPs grown on graphene (NiPt/graphene) have been facilely prepared via a simple one-step coreduction synthetic route and characterized by transmission electron microscopy, energy-dispresive X-ray spectroscopy, X-ray diffraction, inductively coupled plasma atomic emission spectroscopy, X-ray photoelectron spectroscopy, Raman and Fourier transform infrared methods. The characterized results showed that ultrafine Ni–Pt NPs with a small size of around 2.3 nm were monodispersed on the graphene nanosheet. Compared to the pure $Ni_{0.9}Pt_{0.1}$ alloy NPs, graphene supported $Ni_{0.9}Pt_{0.1}$ alloy NPs exhibited much higher activity and hydrogen selectivity (100%) toward conversion of hydrazine borane (HB) to hydrogen. It is first found that the durability of the catalyst can be greatly enhanced by the addition of an excess amount of NaOH in this reaction, because of the neutralization of NaOH by the byproduct H_3BO_3 produced from the hydrolysis of HB. After six cycles of the catalytic reaction, no appreciable decrease in activity was observed, indicating that the $Ni_{0.9}Pt_{0.1}$/graphene catalysts have good durability/stability.

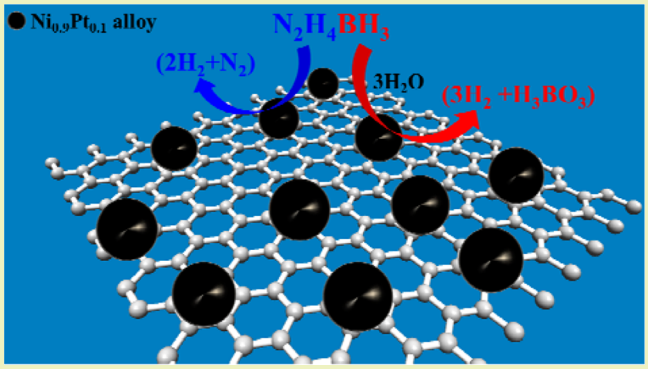

KEYWORDS: *$N_2H_4BH_3$, H_2, NaOH, H_3BO_3, Hydrolysis, Decompose, Neutralization, Durability*

INTRODUCTION

The development of new hydrogen-storage materials that can be used in automotive application is one of the critical issues in the increasing worldwide demand for clean energy sources.[1] Hydrazine borane (HB, $N_2H_4BH_3$) is considered as a promising hydrogen storage material due to its high hydrogen content (15.4 wt %) and safe storability. It can be easily prepared from a reaction of hydrazine hemisulfate with sodium borohydride in dioxane.[2−8] The completely conversion of HB to H_2 via the hydrolysis of BH_3 (eq 1), and the decomposition of N_2H_4 (eqs 2 and 3).[9,10] This corresponds to a theoretical gravimetric hydrogen storage capacity (GHSC) of 10.0 wt % for the system HB–$3H_2O$, which is much higher than those of $NaBH_4$–$4H_2O$ (7.3 wt %) and NH_3BH_3–$4H_2O$ (5.9 wt %). However, hydrolysis of BH_3 proceeds fast and can be easily achieved by non-noble metal-based catalysts,[11,12] whereas decomposition of N_2H_4 via eq 2 is much slower even in the presence of noble-metal catalysts.

$$N_2H_4BH_3(s) + 3H_2O(l) \rightarrow N_2H_4(l) + H_3BO_3(l) + 3H_2(g) \quad (1)$$

$$N_2H_4(l) \rightarrow N_2(g) + 2H_2(g) \quad (2)$$

$$3N_2H_4(l) \rightarrow 4NH_3(g) + N_2(g) \quad (3)$$

To maximize the application of HB as a hydrogen storage material, one must avoid the undesired reaction from eq 3. However, although almost 100% selectivity has been achieved by several catalysts,[13,14] the catalytic kinetics via the decomposition of N_2H_4 is still terribly sluggish or the use of a noble metal is too much for the practical application of this system. Therefore, the development of highly active, low cost, and stable catalysts remains challenging, but is crucial for promoting the practical application of HB as a hydrogen storage material.

It was previously reported that nickel-based nanoparticles (NPs), especially those combined with Pt, Ir and Rh, were active for the hydrogen generation from HB.[10,14−16] To optimize their catalytic performance, effectively controlling the size and dispersion of the active metal NPs is essential. Hence, applicable supports have been designed for controlling the size and restraining the agglomeration of metal NPs. Graphene, as a single-layer of sp^2 carbon material,[17] holding many advantages such as outstanding charge carrier mobility,[18]

Received: March 26, 2015
Revised: April 27, 2015
Published: April 30, 2015

DOI: 10.1021/acssuschemeng.5b00250
ACS Sustainable Chem. Eng. 2015, 3, 1255−1261

fantastic thermal and chemical stability,[19] superior electrical conductivity,[20] etc., and thus could be applied in electronics, engineering materials as well as an ideal substrate for high-performance catalysts.[21−23] It is known that the enhanced catalytic activity of the graphene supported metal NPs is mainly caused by the charge transfer across the graphene−metal surface, due to the Fermi level difference and graphene−metal spacing.[24] Although many studies have focused on graphene-based materials, the task of direct growth and anchoring of metal NPs on graphene with a narrow size distribution and high dispersity and then greatly improving their catalytic activity is still full of challenges.[21,25]

Herein, we report a mild and rapid strategy for one-step synthesis of graphene-supported ultrafine monodispersed Ni−Pt alloy NPs (~2.3 nm). In comparison with the $Ni_{0.9}Pt_{0.1}$ alloy NPs, Ni- and Pt/graphene catalysts, the $Ni_{0.9}Pt_{0.1}$/graphene catalyst with low noble-metal content exhibited a superior catalytic activity with 6.0 equiv (H_2 + N_2) per HB released and a high turnover frequency (TOF) value of 240 h^{-1} (mol_{H2}·mol_{metal}·h^{-1}). In addition, this special catalyst presented a sustainable selectivity and activity after six cycles of reactions. The improvement of catalytic activity and stability of NiPt/graphene can be ascribed to the strong interaction between the active metal NPs and graphene, and the promoting effect of NaOH.

EXPERIMENTAL SECTION

Materials. Potassium tetrachloroplatinate(II) (K_2PtCl_4, 99.95%), 1,4-dioxane (99.8%) and sodium borohydride ($NaBH_4$, 98%) were purchased from J&K Chemical. Hydrazine hemisulfate salt (N_2H_4·1/$2H_2SO_4$) and *n*-pentane (99.5%) were obtained from Sigma-Aldrich. Hexadecyltrimethylammonium bromide-aided (CTAB, $CH_3(CH_2)_{15}N(Br)(CH3)_3$, ≥96.0%) was bought from Fluka. Nickel(II) chloride hexahydrate ($NiCl_2$·$6H_2O$, ≥98.0%), NaOH (≥96.0%) and hydrochloric acid (HCl, 36−37%) were purchased from Sinopharm Chemical Reagent Co., Ltd. Ordinary distilled water was used as the reaction solvent.

Instrumentation. The purity of the as-synthesized HB was determined by a Bruker 400 M liquid ^1H NMR instrument using CD_3CN as the solvent. The chemical compositions of all the $Ni_{1-x}Pt_x$/graphene catalysts were determined by using a 725-ES inductively coupled plasma atomic emission spectroscopy (ICP-AES) instrument. Powder X-ray diffraction (PXRD) studies were performed on a Rigaku RINT-22005 X-ray diffractometer with a Cu Kα source (40 kV, 20 mA). The morphologies and sizes of catalysts were observed by using a transmission electron microscopy (TEM, JEM-2010) instrument equipped with an energy dispersive X-ray (EDX) detector. The TEM samples were prepared by depositing one or two droplets of the synthesized catalyst suspensions on to the amorphous carbon coated copper grids. X-ray photoelectron spectroscopy (XPS) measurement was performed with a Thermo Scientific-ESCALAB 250XI multifunctional imaging electron spectrometer. Raman spectrometry was carried out using a confocal Raman microscope (LabRAM HR). Fourier transform infrared (FTIR) spectra were collected at room temperature by using a Thermo Nicolet 870 instrument using KBr discs in the 500−4000 cm^{-1} region. Mass analysis of the generated gases was performed using a Balzers Prisma QMS 200 mass spectrometer.

Synthesis of HB. HB was synthesized according to the previous reports.[5,12] Typically, 80 mL of anhydrous dioxane containing 21.42 g of hydrazine hemisulfate salt (N_2H_4·1/$2H_2SO_4$) and 10 g of sodium borohydride ($NaBH_4$) was stirred at room temperature under an atmosphere of dry argon for 48 h. The resulting slurry was immediately subjected to 12 min of centrifugation at 12000 rpm to get the clear solution. Then, the filtrate was evaporated by a vacuum dryer at 40 °C overnight to get the raw HB, which was further washed with *n*-pentene. The resulting product is a white solid with a purity of 99.2% verified by PXRD (see Figure S1 of the Supporting Information) and ^1H NMR (see Figure S2 of the Supporting Information). ^1H NMR (δ/ppm, probe head Dual $^1H/^{13}C$, 300.13 MHz, CD_3CN, 30 °C, *J*/Hz): 5.45 (s, 2H, B−NH_2), 3.44 (s, 2H, N−NH_2), 1.42 (q, 3H, $^1J_{HB}$ = 95 Hz).

Synthesis of $Ni_{1-x}Pt_x$/Graphene Catalysts. $Ni_{1-x}Pt_x$/graphene catalysts were prepared as a black suspension using a surfactant (hexadecyltrimethylammonium bromide, CTAB) aided coreduction process. Typically, 10 mg of graphene oxide (GO) synthesized by a modified Hummers method[26,27] and 15 mg of CTAB were suspended in 5 mL distilled water under vigorous stirring for 15 min, and then sonicated for 20 min to obtain a well dispersed GO suspension. Then, 21.4 mg of $NiCl_2$·$6H_2O$ and 4.2 mg of $KPtCl_4$ were poured into the solution, and the mixture was keep stirring for 30 min. Afterward, 30 mg of $NaBH_4$ was added with vigorous magnetic stirring for about 20 min, resulting in the generation of the $Ni_{0.9}Pt_{0.1}$/graphene nanocatalyst as a black suspension. The synthesis of other $Ni_{1-x}Pt_x$/graphene nanocatalysts with different Pt molar content (x = 0, 0.3, 0.5, 0.7, 0.9, 1.0) followed the same process.

Synthesis of $Ni_{0.9}Pt_{0.1}$ NPs. $Ni_{0.9}Pt_{0.1}$ NPs were synthesized as follows: 21.4 mg of $NiCl_2$·$6H_2O$ and 4.2 mg of $KPtCl_4$ were added to 5 mL aqueous solution containing 15 mg of CTAB. After the solution was stirred for 30 min, 30 mg of $NaBH_4$ was added with vigorous magnetic stirring for about for 20 min, resulting in the generation of $Ni_{0.9}Pt_{0.1}$ NPs.

Synthesis of Graphene. Graphene was obtained by a reduction of GO with $NaBH_4$. 10 mg of GO was added into 5 mL of distilled water under vigorous stirring for 15 min and then sonicated for 20 min to obtain a well dispersed GO suspension. Then, 30 mg of $NaBH_4$ was added with vigorous magnetic stirring for about 20 min to get the graphene.

Catalysis. The catalytic activity of the as-synthesized $Ni_{1-x}Pt_x$/graphene, $Ni_{0.9}Pt_{0.1}$ and graphene toward hydrogen evolution from HB was evaluated in a typical water-filled graduated burette system (see Scheme S1 of the Supporting Information). Simply, the reactor containing the as-synthesized catalyst suspension (5 mL) with 0.5 M NaOH was placed in a water bath thermostated at 50 °C and connected to a water-filled inverted burette. To eliminate the influence of any evolving ammonia (NH_3), a trap filled with HCl (0.1 M) solution is placed between the reactor and the inverted burette. The flask was well sealed with a silicon septum. A magnetic stirring apparatus was used in our experiments and the stirring rate was fixed at the value of 500 rpm. Then, hydrazine borane [(Ni + Pt)/HB = 0.1] was poured into the reactor and the volume of H_2 along N_2 was measured, from which the molar ratio of $\lambda = n(H_2 + N_2)/n(HB)$ was obtained. The selectivity of hydrogen (α) was evaluated on the basis of the eq (4): $N_2H_4BH_3 + 3H_2O \rightarrow H_3BO_3 + (3 + 2\alpha)H_2 + (2\alpha + 1)/3N_2 + 4(1 - \alpha)/3NH_3$, which could be deduced from eqs 1, 2 and 3. Therefore, the selectivity is defined as follows:

$$\alpha = \frac{3\lambda - 10}{8}\left[\lambda = \frac{n(H_2 + N_2)}{n(HB)}\left(\frac{10}{3} \le \lambda \le 6\right)\right]$$

Durability of $Ni_{0.9}Pt_{0.1}$/Graphene. The durability of the $Ni_{0.9}Pt_{0.1}$/graphene catalyst was tested as follows: after the first cycle of hydrogen generation reaction was completed, another equivalent of HB was subsequently added to the reaction system containing excess amount of NaOH (2.0 M) and the gas released was monitored by the gas burette. The reactions were repeated for six times under the same conditions as the first cycle. The catalysts were finally separated from the reaction solution by centrifugation, washed by water and dried in a vacuum oven.

RESULTS AND DISCUSSION

Synthesis and Characterization of the Catalysts. In a typical synthesis route, ultrafine Ni−Pt alloy NPs immobilized on the graphene nanosheet (NiPt/graphene) were facilely synthesized by coreduction of the metal precursors and GO nanosheet in the presence of CTAB. The morphology and size of as-synthesized nanomaterials were characterized by using

DOI: 10.1021/acssuschemeng.5b00250
ACS Sustainable Chem. Eng. 2015, 3, 1255−1261

TEM. It can be seen from Figure 1a,b of $Ni_{0.9}Pt_{0.1}$/graphene that $Ni_{0.9}Pt_{0.1}$ NPs with an average particle size of about 2.3 nm

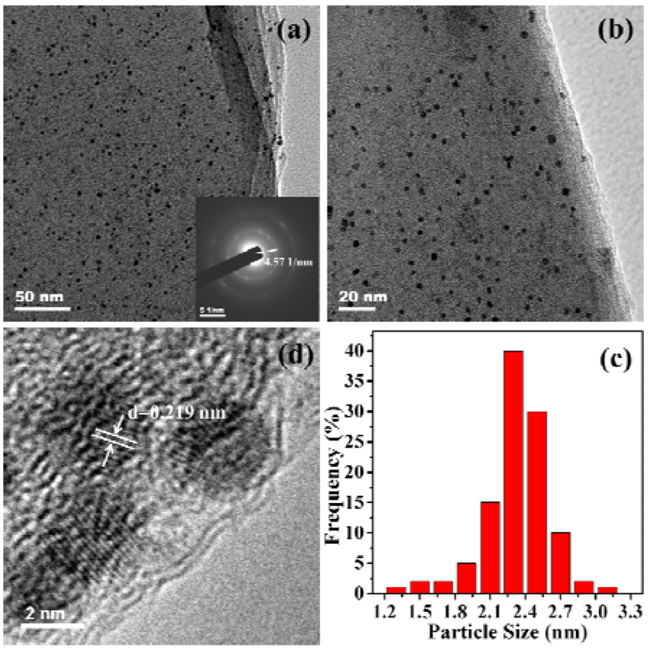

Figure 1. (a,b) Typical TEM and (c) high resolution TEM images images of the $Ni_{0.9}Pt_{0.1}$/graphene catalyst. (d) Size distribution of $Ni_{0.9}Pt_{0.1}$/graphene catalyst. (inset a) Corresponding SAED pattern of $Ni_{0.9}Pt_{0.1}$/graphene catalyst.

(Figure 1d) are monodispersed on the graphene nanosheet. But conversely, the bimetal NPs without graphene are aggregated to larger particles (~5 nm, see Figure S3 of the Supporting Information). The relative smaller particle size and lack of agglomeration of $Ni_{0.9}Pt_{0.1}$/graphene indicates that graphene can successfully serve as not only an excellent support but also an effective dispersing agent for the synthesis of Ni−Pt NPs in aqueous solution. This is due to the fact that the hydrophobic basal plane along with the hydrophilic phenyl epoxide and hydroxyl of GO play a role as a surfactant,[28,29] which can anchor Ni−Pt NPs and thus control their sizes and distribution on graphene sheet during the synthetic process. In addition, the *d*-spacing of the particle was measured to be 0.219 nm from a high resolution TEM image (Figure 1c), which differs from the (111) plane of Ni (0.204 nm) and Pt (0.227) nm, thus indicating that the Ni−Pt NPs are in crystalline alloy state. This is further confirmed by the corresponding selected area energy dispersion (SAED) pattern (inset of Figure 1a), from which the diffraction rings of crystalline Ni−Pt alloy is found. The EDX result (see Figure S4 of the Supporting Information) confirms that Ni and Pt are the main components of the metal NPs. The contents of Ni and Pt were further determined by ICP-AES (shown in Table 1), quite close to the initial amount of Ni and Pt.

The PXRD patterns of the as-synthesized GO, graphene, Ni/graphene, Pt/graphene and $Ni_{0.9}Pt_{0.1}$/graphene samples are shown in Figure 2. In contrast to the characteristic diffraction peak of the as-synthesized GO, the peak at around $2\theta = 10.2°$ corresponds with the (001) reflection of GO disappeared and a new peak at $2\theta = 22.5°$ corresponds with the (002) reflection of graphene was observed in the graphene, Ni/graphene, Pt/graphene and $Ni_{0.9}Pt_{0.1}$/graphene samples, indicating that the

Table 1. Catalysts Composition Determined by Inductively Coupled Plasma Atomic Emission Spectroscopy (ICP-AES)

catalysts	Ni (wt %)	Pt (wt %)	Ni/Pt (molar ratio)
$Ni_{0.9}Pt_{0.1}$/graphene	30.4	12.5	0.89/0.11
$Ni_{0.7}Pt_{0.3}$/graphene	20.2	27.4	0.71/0.29
$Ni_{0.5}Pt_{0.5}$/graphene	12.8	40.8	0.51/0.49
$Ni_{0.3}Pt_{0.7}$/graphene	6.5	52.8	0.29/0.71
$Ni_{0.1}Pt_{0.9}$/graphene	1.5	57.3	0.08/0.92
Ni/graphene	33.3		
Pt/graphene		60.1	

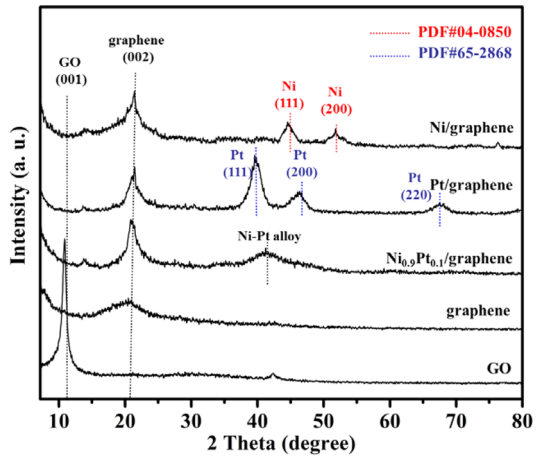

Figure 2. PXRD patterns of the as-synthesized GO, graphene, Ni/graphene, Pt/graphene and $Ni_{0.9}Pt_{0.1}$/graphene samples.

GO nanosheets were successfully reduced to the graphene nanosheets. As shown in Figure 2, $Ni_{0.9}Pt_{0.1}$/graphene exhibits an obvious crystalline peak centered at 41.5°, which is between the fcc (111) diffraction peaks of nickel (PDF#04-0850) and platinum (PDF#65-2868), indicating the formation of Ni−Pt alloy NPs.

It can be seen from Raman spectra (Figure 3a) that the as-synthesized GO and $Ni_{0.9}Pt_{0.1}$/graphene have two peaks centered at 1347 and 1600 cm^{-1}, corresponding to the D and G bands of carbon products.[30,31] The intensity ratio of the D to G bands (I_D/I_G) increases from 1.11 for GO to 1.31 for $Ni_{0.9}Pt_{0.1}$/graphene, indicating that the $Ni_{0.9}Pt_{0.1}$/graphene contains more disordered carbon than GO. Figure 3b shows the FTIR spectra of GO and $Ni_{0.9}Pt_{0.1}$/graphene. It can be seen clearly that the C═O peak at 1634 cm^{-1}, the C—OH peak at 1227 cm^{-1} and the C—O peak at 1057 cm^{-1} of GO disappeared after the formation of graphene supported $Ni_{0.9}Pt_{0.1}$ NPs, further indicating the reduction of GO to graphene during the synthetic process. Additionally, the XPS results for C 1s shows that the intensities of the oxygen containing functional groups (such as −C—O, −C═O, −COO) of GO (Figure 4a,b) decreased significantly after the formation of $Ni_{0.9}Pt_{0.1}$/graphene,[32] which also confirms the reduction of GO during the process. The observed Ni $2p_{3/2}$ and Ni $2p_{1/2}$ with binding energies of 852.8 and 870.2 eV correspond to metallic Ni (Figure 4c), and the Pt $4f_{7/2}$ and Pt $4f_{5/2}$ peaks with binding energy of 70.6 and 73.9 eV correspond to metallic Pt (Figure 4d). The formation of oxidized Ni observed in Ni 2p band, most likely occurs during the sample preparation process for the XPS measurements,[9,10,14,33] can be readily removed by Ar sputtering in 60 s.

DOI: 10.1021/acssuschemeng.5b00250
ACS Sustainable Chem. Eng. 2015, 3, 1255−1261

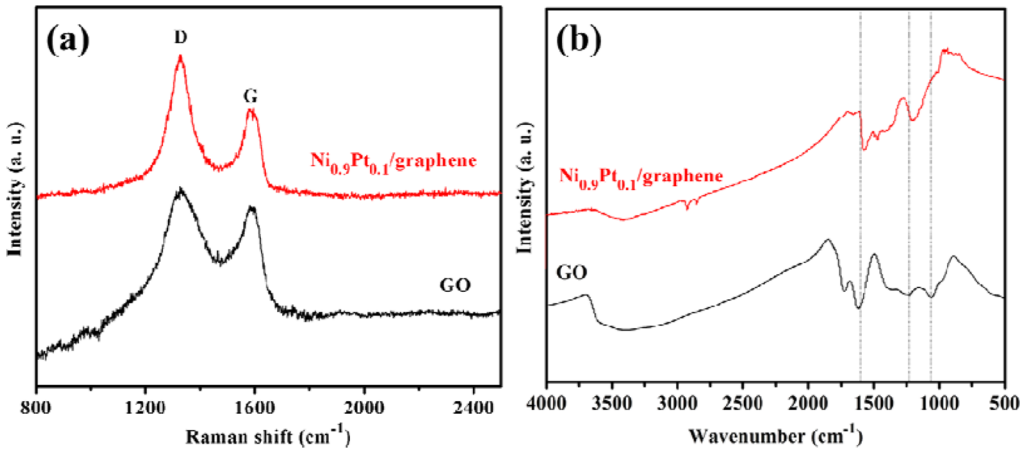

Figure 3. (a) Raman spectra of the GO and $Ni_{0.9}Pt_{0.1}$/graphene sample; (b) FTIR spectra of the GO and $Ni_{0.9}Pt_{0.1}$/graphene sample.

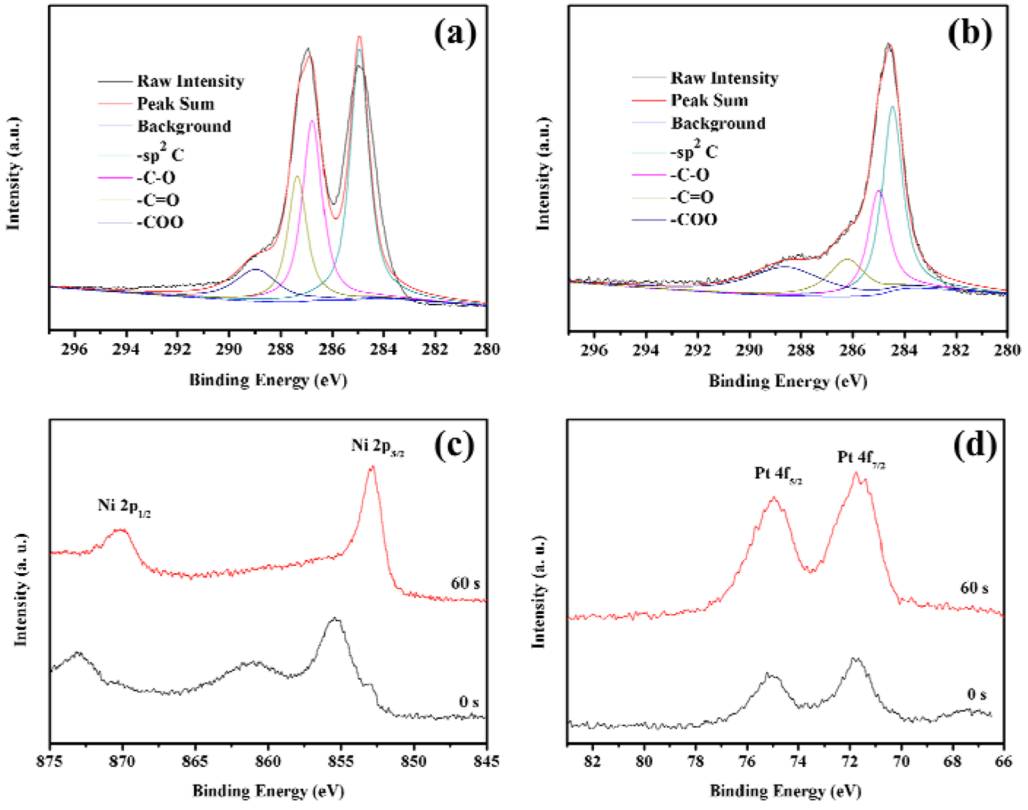

Figure 4. XPS spectra of (a) C 1s of GO; (b) C 1s of $Ni_{0.9}Pt_{0.1}$/graphene; (c) Ni 2p and (d) Pt 4f of $Ni_{0.9}Pt_{0.1}$/graphene catalyst before and after argon sputtering for 60 s.

Catalytic Performance. Catalytic activities of the as-synthesized $Ni_{1-x}Pt_x$/graphene catalysts with various contents of Ni−Pt together with their bicounterparts (Ni/graphene and Pt/graphene) have been investigated for the hydrogen generation from HB at 323 K in the presence of NaOH (0.5 M), as shown in Figure 5. It is clear that, compared to their monometallic Ni/graphene or Pt/graphene catalysts, alloying a small amount of Pt to Ni can significantly enhance the catalytic activity and selectivity. Among these catalysts, the bimetallic $Ni_{0.9}Pt_{0.1}$/graphene catalyst exhibits the highest catalytic performance. $Ni_{0.9}Pt_{0.1}$/graphene can completely convert the hydrogen of HB to H_2 with 6.0 equiv (H_2 + N_2) per HB released in only 12.5 min, which confirms that the resulting synergistic effect between Ni and Pt is required for hydrogen generation from HB.[34−37] The TOF of $Ni_{0.9}Pt_{0.1}$/graphene is calculated to be 240 h^{-1} ($mol_{H2}{\cdot}mol_{metal}{}^{-1}{\cdot}h^{-1}$), relatively high values in the reported catalysts for hydrogen generation from HB at the same reaction conditions (see Table S1 of the Supporting Information). The H_2/N_2 ratio of the gases released from HB over $Ni_{0.9}Pt_{0.1}$/graphene was further confirmed by the mass spectrometric analysis (see Figure S5 of the Supporting Information).

For comparison, the catalytic performances of the as-synthesized graphene, $Ni_{0.9}Pt_{0.1}$ alloy NPs and $Ni_{0.9}Pt_{0.1}$/graphene catalysts for the hydrogen generation from HB are presented in Figure 6. No activity is observed for graphene toward this reaction. For $Ni_{0.9}Pt_{0.1}$, 5.47 equiv (H_2 + N_2) per HB is released in 35.6 min, and its TOF value is only 77.5 h^{-1}.

DOI: 10.1021/acssuschemeng.5b00250
ACS Sustainable Chem. Eng. 2015, 3, 1255−1261

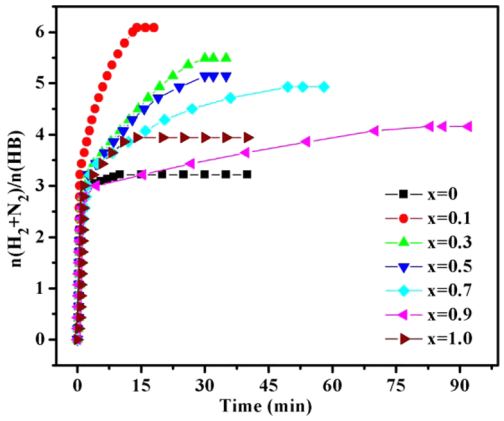

Figure 5. Time course plots for hydrogen generation from HB (200 mM, 5 mL) over $Ni_{1-x}Pt_x$/graphene catalysts ((Ni + Pt)/(HB) = 0.1) with NaOH (0.5 M) at 323 K.

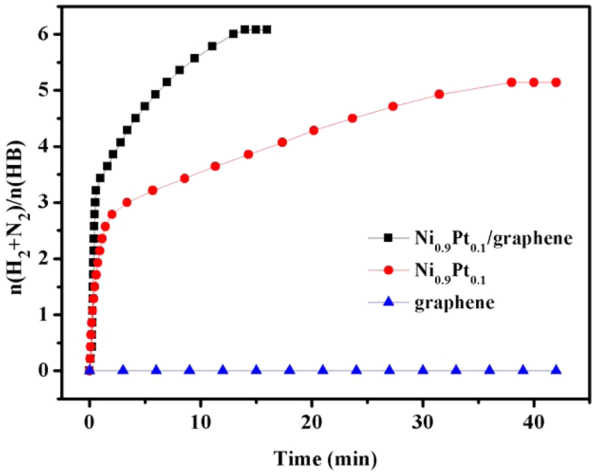

Figure 6. Time course plots for hydrogen generation from HB (200 mM, 5 mL) over $Ni_{0.9}Pt_{0.1}$/graphene, $Ni_{0.9}Pt_{0.1}$ NPs ((Ni + Pt)/(HB) = 0.1) and graphene with NaOH (0.5 M) at 323 K.

Clearly, $Ni_{0.9}Pt_{0.1}$/graphene exhibits much higher activity and selectivity than that of pure $Ni_{0.9}Pt_{0.1}$ alloy NPs. The enhanced catalytic activity of $Ni_{0.9}Pt_{0.1}$/graphene for hydrogen generation from HB is probably due to the significant synergistic effect between $Ni_{0.9}Pt_{0.1}$ NPs and graphene sheet. The narrow particle size distribution and high dispersity of $Ni_{0.9}Pt_{0.1}$ NPs supported on graphene also plays an important role in promoting the catalytic performance.

Previous research has shown that the presence of NaOH played an important role in promoting the catalytic performance for decomposition of hydrous hydrazine.[21,39] For $Ni_{0.9}Pt_{0.1}$/graphene without NaOH, only 4.9 equiv (H_2 + N_2) per HB released in 50 min with a TOF value of 50.4 h^{-1}. However, the addition of NaOH to the reaction system can significantly enhance the catalytic performance of $Ni_{0.9}Pt_{0.1}$/graphene (Figure 7). It can be seen from Figure 7 that the ratio of $n(H_2 + N_2)/n(HB)$ markedly increases from 4.9 to 6.0 when the concentration of NaOH changes from 0 to 0.5 M, and the ratio of $n(H_2 + N_2)/n(HB)$ will not change with the further increase of NaOH concentration to 0.9 M. These results indicate that the optimized NaOH concentration for this catalytic system is 0.5 M (Figure 7). In addition, the similarity in catalytic performance with KOH or NaOH indicates that the promotion effect of alkaline is general instead of alkali type-

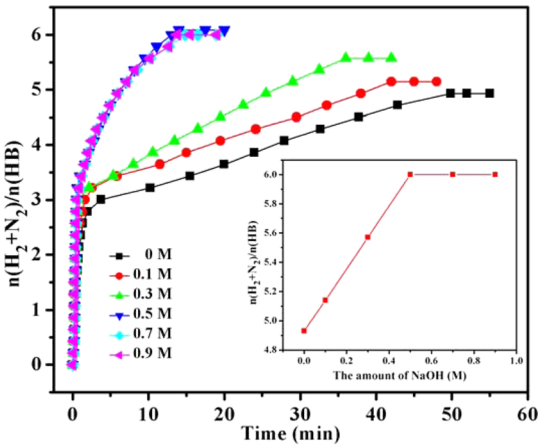

Figure 7. Time course plots for hydrogen generation from HB (200 mM, 5 mL) over $Ni_{0.9}Pt_{0.1}$/graphene catalyst ((Ni + Pt)/(HB) = 0.1) with different molar concentrations of NaOH at 323 K.

dependent (see Figure S6 of the Supporting Information). It has been known that NaOH or KOH here only serves as a catalyst promoter for the decomposition of the N_2H_4 moiety. This is understandable because the existence of OH^- can decrease the concentration of $N_2H_5^+$ ($N_2H_5^+ + OH^- \rightarrow N_2H_4 + H_2O$) in aqueous solution and also promote the rate-determing deprotonation step ($N_2H_4 \rightarrow N_2H_3^* + H^*$) along the decomposition process of N_2H_4 to H_2 and N_2.[38] Besides promoting the reaction kinetics, the alkaline solution can also help to prevent the formation of NH_3 and thereby could increase the hydrogen selectivity.[39]

After finished the first cycle of hydrogen generation reaction in the presence of 0.5 M NaOH, it is easy to find that the catalytic activity of $Ni_{0.9}Pt_{0.1}$/graphene decreased significantly in the second cycle when directly adding the same amount of HB to the reactor without addition of NaOH (Figure 8a). But when the catalyst was washed after the first cycle of reaction and reused at the same conditions with addition of 0.5 M NaOH, the activity and selectivity of catalyst did not decrease (Figure 8b). Figure S7 of the Supporting Information shows the TEM images of the $Ni_{0.9}Pt_{0.1}$/graphene after hydrogen release with or without addition of NaOH (see the Supporting Information). Both of them have similar particle size and dispersity, although the size of some particles became a little bigger in comparison with the fresh sample before reaction. Therefore, size effect can be excluded for the samples during the recycle test with and without addition of NaOH.

To find the real answer for the decrease of activity, we checked the reaction solutions. The pH values of the reaction solution before and after the first cycle of reaction were measured to be 13.69 and 12.82 (the concentration of OH^{-1} decreased from 0.5 to 0.07 M), respectively, due to the neutralization of NaOH by the resulting H_3BO_3 produced from the first hydrolysis step. Therefore, the decrease pH value of the reaction solution will lead to a decrease in catalytic activity and selectivity in the second cycle of test. Herein, a very important detail that needs to be mentioned is that, an excess amount of NaOH (2.0 M) should be added before the durability test to eliminate the negative influence of the decrease pH value, although the optimized NaOH concentration in the previous test is 0.5 M (Figure 7). Figure 9 shows the yield of equiv. (H_2 + N_2) per HB versus time graph for hydrogen generation from HB at sequential runs in the presence of 2.0 M NaOH. After

DOI: 10.1021/acssuschemeng.5b00250
ACS Sustainable Chem. Eng. 2015, 3, 1255−1261

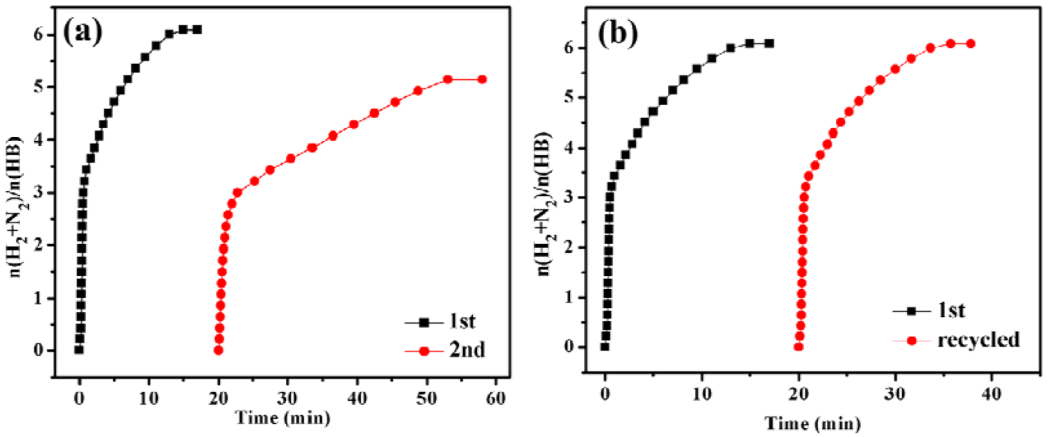

Figure 8. Time course plots for hydrogen generation from HB (200 mM, 5 mL) over $Ni_{0.9}Pt_{0.1}$/graphene ((Ni + Pt)/(HB) = 0.1, 0.5 M NaOH, 323 K) at sequential runs by (a) directly adding equivalent molar amounts of HB into the reactor and (b) reusing the catalyst after washing by water with addition of equivalent molar amounts of HB and 0.5 M NaOH.

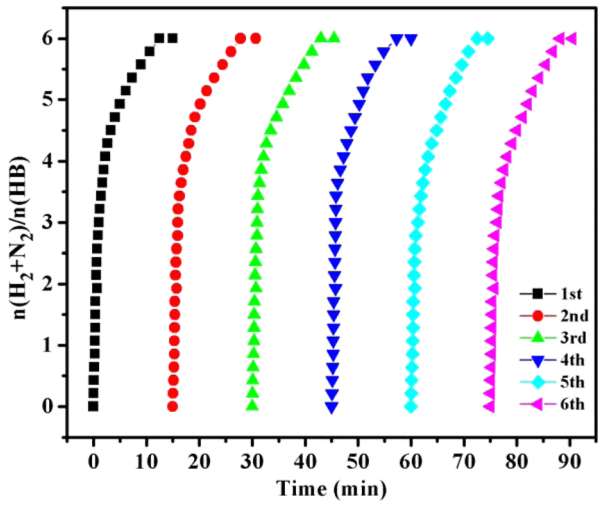

Figure 9. Time course plots for hydrogen generation from HB (200 mM, 5 mL) over $Ni_{0.9}Pt_{0.1}$/graphene catalyst ((Ni + Pt)/(HB) = 0.1, 2.0 M NaOH, 323 K) at sequential runs by the addition of equivalent molar amounts of HB.

the six successive runs, the activity of the catalysts has no obvious decrease and the yield of equiv. (H_2 + N_2) per HB keeps at the value of 6.0, indicating that the $Ni_{0.9}Pt_{0.1}$/graphene has good durability for hydrogen generation from HB aqueous solution in the presence of an excess amount of NaOH (2.0 M). For the first time, it is found that the durability of the catalyst can be significantly enhanced by the addition of an excess amount of NaOH in hydrogen generation from HB. The good stability of the $Ni_{0.9}Pt_{0.1}$/graphene can be confirmed by TEM characterization. In contrast to the fresh synthesized $Ni_{0.9}Pt_{0.1}$/graphene sample, the TEM image of $Ni_{0.9}Pt_{0.1}$/graphene after six runs of durability test exhibits that the bimetal nanoparticles are still well dispersed on the graphene and no obvious agglomeration is observed (see Figure S8 of the Supporting Information).

In addition, the effect of stirring rate for catalytic activity and durability of $Ni_{0.9}Pt_{0.1}$/graphene was investigated. As shown in Figure S9 of the Supporting Information, the TOF is 120 h^{-1} without magnetic stirring. The TOF value increased from 240 to 280 h^{-1}, with the stirring rate increased from 500 to 1500 rpm. As for durability test of $Ni_{0.9}Pt_{0.1}$/grapheme, there is only a small decrease after six runs with or without magnetic stirring.

CONCLUSIONS

In summary, graphene-supported ultrafine monodispersed Ni–Pt alloy NPs were facilely and successfully prepared by a one-step coreduction strategy, and were tested as catalysts for hydrogen generation from alkaline solution of HB. The graphene was proved to be not only a distinct support but also an efficient dispersing agent for the synthesis of Ni–Pt NPs in aqueous solution. The obtained $Ni_{0.9}Pt_{0.1}$/graphene catalyst with a low noble-metal content exerts excellent catalytic performance for complete conversion of HB to H_2 and N_2 at 323 K. The catalytic activity and selectivity of the catalyst in the cycle test can be significantly enhanced by the addition of an excess amount of NaOH. High activity (240 h^{-1}) and hydrogen selectivity (100%), and excellent durability were achieved in the present work. The obtained excellent catalytic performance of this special catalyst may promote the practical application of HB for chemical hydrogen storage.

ASSOCIATED CONTENT

Supporting Information

Additional information as noted in text. The Supporting Information is available free of charge on the ACS Publications website at DOI: 10.1021/acssuschemeng.5b00250.

AUTHOR INFORMATION

Corresponding Author

*E-mail: luzh@jxnu.edu.cn (Z.-H. Lu).

Notes

The authors declare no competing financial interest.

ACKNOWLEDGMENTS

This work was financially supported by National Natural Science Foundation of China (No. 21463012 and 21103074). Z. Z. was supported by Scientific Research Foundation of Graduate School of Jiangxi Normal University (YJS2014054). Z.-H. Lu was supported by Young Scientist Foundation of Jiangxi Province (20133BCB23011), and "Gan-po talent 555" Project of Jiangxi Province.

DOI: 10.1021/acssuschemeng.5b00250
ACS Sustainable Chem. Eng. 2015, 3, 1255–1261

REFERENCES

(1) Schlapbach, L.; Züttel, A. Hydrogen-storage materials for mobile applications. *Nature* **2001**, *414*, 353−358.

(2) Goubeau, J.; Ricker, E. Borinhydrazin und seine pyrolyseprodukte. *Z. Anorg. Allg. Chem.* **1961**, *310*, 123−142.

(3) Gunderloy, F. C., Jr. Reaction of the borohydride group with the proton donors hydroxylammonium, methoxyammonium, and hydraziniummagnesium ions. *Inorg. Chem.* **1963**, *2*, 221−222.

(4) Hügle, T.; Kühnel, M. F.; Lentz, D. Hydrazine borane: A promising hydrogen storage material. *J. Am. Chem. Soc.* **2009**, *131*, 7444−7446.

(5) Moury, R.; Moussa, G.; Demirci, U. B.; Hannauer, J.; Bernard, S.; Petit, E.; Lee, A.; Miele, P. Hydrazine borane: Synthesis, characterization, and application prospects in chemical hydrogen storage. *Phys. Chem. Chem. Phys.* **2012**, *14*, 1768−1777.

(6) Vinh-Son, N.; Swinnen, S.; Lesczynski, J.; Nguyen, M. T. Formation and hydrogen release of hydrazine bisborane: Transfer vs. attachment of a borane. *Phys. Chem. Chem. Phys.* **2011**, *13*, 6649−6656.

(7) Karahan, S.; Zahmakıran, M.; Özkar, S. Catalytic hydrolysis of hydrazine borane for chemical hydrogen storage: Highly efficient and fast hydrogen generation system at room temperature. *Int. J. Hydrogen Energy* **2011**, *36*, 4958−4966.

(8) Thomas, J.; Klahn, M.; Spannenberg, A.; Beweries, T. Group 4 metallocene catalyzed full dehydrogenation of hydrazine borane. *Dalton Trans.* **2013**, *42*, 14668−14672.

(9) Hannauer, J.; Akdim, O.; Demirci, U. B.; Geantet, C.; Herrmann, J. M.; Miele, P.; Xu, Q. High-extent dehydrogenation of hydraizne borane $N_2H_4BH_3$ by hydrolysis of BH_3 and decomposition of N_2H_4. *Energy Environ. Sci.* **2011**, *4*, 3355−3358.

(10) Zhong, D. C.; Aranishi, K.; Singh, A. K.; Demirci, U. B.; Xu, Q. The synergistic effect of Rh-Ni catalysts on the highly-efficient dehydrogenation of aqueous hydrazine borane for chemical hydrogen storage. *Chem. Commun.* **2012**, *48*, 11945−11947.

(11) Ben Aziza, W.; Petit, J. F.; Demirci, U. B.; Xu, Q.; Miele, P. Bimetallic nickel-based nanocatalysts for hydrogen generation from aqueous hydrazine borane: Investigation of iron, cobalt and palladium as the second metal. *Int. J. Hydrogen Energy* **2014**, *39*, 16919−16926.

(12) Yao, Q.; Lu, Z. H.; Zhang, Z.; Chen, X.; Lan, Y. One-pot synthesis of core-shell $Cu@SiO_2$ nanospheres and their catalysis for hydrolytic dehydrogenation of ammonia borane and hydrazine borane. *Sci. Rep.* **2014**, *4*, 7597 DOI: 10.1038/srepo7597.

(13) Zhu, Q. L.; Zhong, D. C.; Demirci, U. B.; Xu, Q. Controlled synthesis of ultrafine surfactant-free NiPt nanocatalysts toward efficient and complete hydrogen generation from hydrazine borane at room temperature. *ACS Catal.* **2014**, *4*, 4261−4268.

(14) Çakanyıldırım, Ç.; Demirci, U. B.; Şener, T.; Xu, Q.; Miele, P. Nickel-based bimetallic nanocatalysts in high-extent dehydrogenation of hydrazine borane. *Int. J. Hydrogen Energy* **2012**, *37*, 9722−9729.

(15) Clémençon, D.; Petit, J. F.; Demirci, U. B.; Xu, Q.; Miele, P. Nickel- and platinum-containing core@shell catalysts for hydrogen generation of aqueous hydrazine borane. *J. Power Sources* **2014**, *260*, 77−81.

(16) Li, C.; Dou, Y.; Liu, J.; Chen, Y.; He, S.; Wei, M.; Evans, D. G.; Duan, X. Synthesis of supported Ni@(RhNi-alloy) nanocomposites as an efficient catalyst towards hydrogen generation from $N_2H_4BH_3$. *Chem. Commun.* **2013**, *49*, 9992−9994.

(17) Geim, A. K.; Novoselov, K. S. The rise of graphene. *Nat. Mater.* **2007**, *6*, 183−191.

(18) Lee, C.; Wei, X.; Kysar, J. W.; Hone, J. Measurement of the elastic properties and intrinsic strength of monolayer graphene. *Science* **2008**, *321*, 385−388.

(19) Novoselov, K. S.; Geim, A. K.; Morozov, S. V.; Jiang, D.; Zhang, Y.; Dubonos, S. V.; Grigorieva, I. V.; Firsov, A. A. Electric field effect in atomically thin carbon films. *Science* **2004**, *306*, 666−669.

(20) Choi, B. G.; Hong, J.; Park, Y. C.; Jung, D. H.; Hong, W. H.; Hammond, P. T.; Park, H.-S. Innovative polymer nanocomposite electrolytes: Nanoscale manipulation of ion channels by functionalized graphenes. *ACS Nano* **2011**, *5*, 5167−5174.

(21) Wang, J.; Zhang, X. B.; Wang, Z. L.; Wang, L. M.; Zhang, Y. Rhodium-nickel nanoparticles grown on graphene as highly efficient catalyst for complete decomposition of hydrous hydrazine at room temperature for chemical hydrogen storage. *Energy Environ. Sci.* **2012**, *5*, 6885−6888.

(22) Wang, T.; Li, C.; Ji, J.; Wei, Y.; Zhang, P.; Wang, S.; Fan, X.; Gong, J. Reduced graphene oxide (rGO)/$BiVO_4$ composites with maximized interfacial coupling for visible light photocatalysis. *ACS Sustainable Chem. Eng.* **2014**, *2*, 2253−2258.

(23) Li, L.; Zhang, J.; Liu, Y.; Zhang, W.; Yang, H.; Chen, J.; Xu, Q. Facile fabrication of Pt nanoparticles on 1-pyrenamine functionalized graphene nanosheets for methanol electrooxidation. *ACS Sustainable Chem. Eng.* **2013**, *1*, 527−533.

(24) Guo, S.; Sun, S. FePt nanoparticles assembled on graphene as enhanced catalyst for oxygen reduction reaction. *J. Am. Chem. Soc.* **2012**, *134*, 2492−2495.

(25) Chen, Y.; Zhu, Q. L.; Tsumori, N.; Xu, Q. Immobilizing highly catalytically active noble metal nanoparticles on reduced graphene oxide: A non-noble metal sacrificial approach. *J. Am. Chem. Soc.* **2015**, *137*, 106−109.

(26) Yang, Y.; Lu, Z. H.; Hu, Y.; Zhang, Z.; Shi, W.; Chen, X.; Wang, T. Facile in situ synthesis of copper nanoparticles supported on reduced graphene oxide for hydrolytic dehydrogenation of ammonia borane. *RSC Adv.* **2014**, *4*, 13749−13752.

(27) Kovtyukhova, N. I.; Ollivier, P. J.; Martin, B. R.; Mallouk, T. E.; Chizhik, S. A.; Buzaneva, E. V.; Gorchinskiy, A. D. Layer-by-layer assembly of ultrathin composite films from micron-sized graphite oxide sheets and polycations. *Chem. Mater.* **1999**, *11*, 771−778.

(28) Kim, J.; Cote, L. J.; Kim, F.; Yuan, W.; Shull, K. R.; Huang, J. Graphene oxide sheets at interfaces. *J. Am. Chem. Soc.* **2010**, *132*, 8180−8186.

(29) Jasuja, K.; Berry, V. Implantation and growth of dendritic gold nanostructures on graphene derivatives: Electrical property tailoring and raman enhancement. *ACS Nano* **2009**, *3*, 2358−2366.

(30) Rourke, J. P.; Pandey, P. A.; Moore, J. J.; Bates, M.; Kinloch, I. A.; Young, R. J.; Wilson, N. R. The real graphene oxide revealed: Stripping the oxidative debris from the graphene-like sheets. *Angew. Chem., Int. Ed.* **2011**, *123*, 3231−3235.

(31) Stankovich, S.; Dikin, D. A.; Piner, R. D.; Kohlhaas, K. A.; Kleinhammes, A.; Jia, Y.; Wu, Y.; Nguyen, S.; Ruoff, R. S. Synthesis of graphene-based nanosheets via chemical reduction of exfoliated graphite oxide. *Carbon* **2007**, *45*, 1558−1565.

(32) Yan, J. M.; Wang, Z. L.; Wang, H. L.; Jiang, Q. Rapid and energy-efficient synthesis of a graphene-CuCo hybride as a high performance catalyst. *J. Mater. Chem.* **2012**, *22*, 10990−10993.

(33) Cao, N.; Yang, L.; Dai, H.; Liu, T.; Su, J.; Wu, X.; Luo, W.; Cheng, G. Immobilizing of ultrafine bimetallic Ni-Pt nanoparticles inside the pores of metal-organic frameworks as efficient catalysts for dehydrogenation of alkaline solution of hydrazine. *Inorg. Chem.* **2014**, *53*, 10122−10128.

(34) Bashyam, R.; Zelenay, P. A class of non-precious metal composite catalysts for fuel cells. *Nature* **2006**, *443*, 63−66.

(35) Morozan, A.; Jousselme, B.; Palacin, S. Low-platinum and platinum-free catalysts for the oxygen reduction reaction at fuel cell cathodes. *Energy Environ. Sci.* **2011**, *4*, 1238−1254.

(36) Jiang, H. L.; Xu, Q. Recent progress in synergistic catalysis over heterometallic nanoparticles. *J. Mater. Chem.* **2011**, *21*, 13705−13725.

(37) Singh, A. K.; Xu, Q. Synergistic catalysis over bimetallic alloy nanoparticles. *ChemCatChem* **2013**, *5*, 652−676.

(38) Wang, J.; Li, Y.; Zhang, Y. Precious-metal-free nanocatalysts for highly efficient hydrogen production from hydrous hydrazine. *Adv. Funct. Mater.* **2014**, *24*, 7073−7077.

(39) Singh, S. K.; Singh, A. K.; Aranishi, K.; Xu, Q. Noble-metal-free bimetallic nanoparticle-catalyzed selective hydrogen generation from hydrous hydrazine for chemical hydrogen storage. *J. Am. Chem. Soc.* **2011**, *133*, 19638−19641.

DOI: 10.1021/acssuschemeng.5b00250
ACS Sustainable Chem. Eng. 2015, 3, 1255−1261